Measurement of the Soret coefficient in liquid Al-Ag alloys using x-ray radiography

Asbjørn Torsvik Krüger,* Elke Sondermann, and Andreas Meyer
Institute of Material Physics in Space, German Aerospace Center (DLR), 51147 Cologne, Germany

(Received 2 December 2022; revised 24 January 2023; accepted 2 February 2023; published 15 February 2023)

Thermodiffusion designates a diffusive motion of particles driven by a temperature gradient. In liquid alloys, this effect can influence the concentration distribution during directional solidification and change the homogeneity of grown crystals. Using x-ray radiography (XRR), thermodiffusion in liquid Al–Ag has been measured, with compositions ranging from $Al_{80}Ag_{20}$ to $Al_{50}Ag_{50}$. The Soret coefficient is determined to be $(0.9 \pm 0.3) \times 10^{-3}$ K^{-1}, where the silver atoms diffuse to the cold end of the sample. Thanks to the time-resolved information from *in situ* XRR, the interdiffusion coefficient could simultaneously be measured and is in good agreement with previous interdiffusion measurements in this concentration range. The measured Soret coefficient is compared with the values predicted by the current theoretical models, which are found to be off by at least a factor of two.

DOI: 10.1103/PhysRevB.107.064301

I. INTRODUCTION

Thermodiffusion, also called the Soret effect, is the separation of the components of a mixture toward the hot/cold regions in a nonuniform temperature distribution [1]. The effect is observed to influence all kinds of matter, from gases to liquids to solids [2].

In recent years, thermodiffusion has been studied in organic solutions which is needed for the understanding of natural hydrocarbon reservoirs. To obtain reliable experimental data, several research groups decided to investigate selected sample systems with different methods. In comparing the results, a benchmark for these binary organic solutions was successfully obtained [3]. Measurements of thermodiffusion are easily disturbed by convection [4]. To avoid gravity-induced convection, several thermodiffusion experiments in organic mixtures have been conducted in microgravity aboard the International Space Station [5,6].

In metals, the effect has been employed for nuclear enrichment and crystal growth; it is relevant for solders and manufacturing of integrated circuits and has recently been shown to be of use in creating metallic nanowires [7–12].

There exist several theoretical models attempting to predict binary thermodiffusion, but there is still no comprehensive model that can predict the Soret coefficient for a wider range of systems, as recently shown by Hoang and Galliero [13]. The authors of such models often voice the need for more experimental data [14–17], which is very scarce in the case of metallic melts. The same holds for modeling thermodiffusion using computational simulations, where the dynamics of thermodiffusion in the simulations (dependence of thermodiffusion on mixture size ratio, dependence of Soret coefficient on concentration, etc.) should be compared with measurements [18,19].

Here, we study thermodiffusion in the liquid alloy Al–Ag as a function of composition using a recently developed experimental setup. The addition of silver to several aluminum alloys heightens the strength and hardenability [20]. Almost all previous publications on liquid alloys are on binary systems where the atomic mass ratio of the two components is ∼2 or less, like Bi–Pb, Al–Cu, and Ag–Te [14,21,22]. The only exceptions so far are measurements on carbon and trace amounts in a solvent [23–25]. The experimental data so far indicate that the Soret coefficient is generally dependent on the relative molecular weights of the species in the mixture [1]. Measuring the thermodiffusion in liquid Al–Ag for different concentrations therefore provides insight into the dynamics of thermodiffusion in an atomic fluid with a high mass ratio.

In previous experimental works on binary alloys, closed containers with columns of the liquid were used which were submitted to a thermal gradient for a certain amount of time, then quickly cooled, and finally analyzed in the solid state [22,25,26]. To avoid changes of the concentration gradient during solidification, some experiments instead used a shear cell technique, where the sample is split up in segments after the annealing time while still in the liquid state [27,28]. A drawback of both of these methods is that possible bubbles in the melt cannot be detected. The presence of bubbles may lead to Marangoni convection, which can disturb diffusion measurements [29,30]. Furthermore, it is interesting to note that, in the case of interdiffusion measurements, such bubbles have been shown to increase the apparent interdiffusion coefficient by a factor of two [31]. Recently, *in situ* x-ray radiography (XRR) has been shown to allow time- and space-resolved measurements of thermodiffusion in liquid alloys, where bubbles or free surfaces can be directly detected during the experiment [32]. Using this time-resolved method, it is even possible to determine the interdiffusion coefficient and the Soret coefficient simultaneously. The high mass ratio between Al and Ag proves useful, as this also leads to a high contrast between the two components in the x-ray spectrum.

*asbjorn.krueger@dlr.de

 ©2023 American Physical Society

Using Al–Ag, the liquidus temperature of the eutectic system at 839 K is relatively low [33]. Also, the interdiffusion coefficient for the system has been previously established by Engelhardt *et al.* [34], which provides a reference for validation of the interdiffusion coefficient measured here. Finally, several thermodynamic properties of Al–Ag melts have been studied before which makes it possible to test models for thermodiffusion.

II. THEORY

In a binary mixture, the mass diffusion flux $\mathbf{J}$ is driven by the interdiffusion from a concentration gradient ∇c and the thermodiffusion from a temperature gradient ∇T, given by the equation [35]:

$$\mathbf{J} = -\rho D \nabla c - \rho D_{\mathrm{T}} c_0 (1 - c_0) \nabla T. \tag{1}$$

Here, ρ is the density, D the interdiffusion coefficient, D_{T} the thermodiffusion coefficient, and c_0 the concentration of one of the two species. After the thermal gradient has been applied and the steady state has been reached (i.e., $\mathbf{J} = 0$), the interdiffusion and thermodiffusion processes reach an equilibrium defined by

$$\nabla c = -\frac{D_{\mathrm{T}}}{D} c_0 (1 - c_0) \nabla T, \tag{2}$$

where the ratio between the thermodiffusion and interdiffusion coefficients is called the Soret coefficient $S_{\mathrm{T}} = \frac{D_{\mathrm{T}}}{D}$. For a one-dimensional sample in a linear temperature gradient, the total concentration difference across the sample from the total temperature difference ΔT becomes

$$\Delta c_\infty = -S_{\mathrm{T}} c_0 (1 - c_0) \Delta T \tag{3}$$

after reaching equilibrium.

Equations describing the transient concentration difference as a function of time have been developed in the case of an instantaneously applied temperature gradient ΔT [36–38]. Following the derivations by Costesèque *et al.* [37] and Mialdun and Shevtsova [38], the total concentration difference across the sample over time t is given by the infinite sum:

$$\Delta c(t) = \Delta c_\infty \left\{ 1 - \frac{8}{\pi^2} \sum_{k=0}^{\infty} \frac{\exp[-(2k+1)^2 t/\theta]}{(2k+1)^2} \right\}, \tag{4}$$

where $\theta = \frac{L^2}{\pi^2 D}$ is the characteristic time, and L is the sample length.

III. METHOD

A. Experimental setup

The pure elements (aluminum: abcr GmbH 99.999 %, silver: Alfa Aesar Premion Silver shot 99.99 %) were alloyed in an arc melting furnace under a high-purity argon atmosphere.

The prepared Al–Ag alloys were suction-cast into rods of ∼1.2 mm thickness and subsequently cut to a length of 12.2 mm. The samples were then placed inside 1.3-mm-wide and 12.5-mm-deep borings in the boron nitride (BN) sample cell, where they were melted and analyzed under x-ray illumination. The liquid samples were compressed by BN pistons to limit the presence of bubbles during the filling of the capillary by the liquid. The lengths of the molten samples ranged from 9.5 to 11.5 mm after compression.

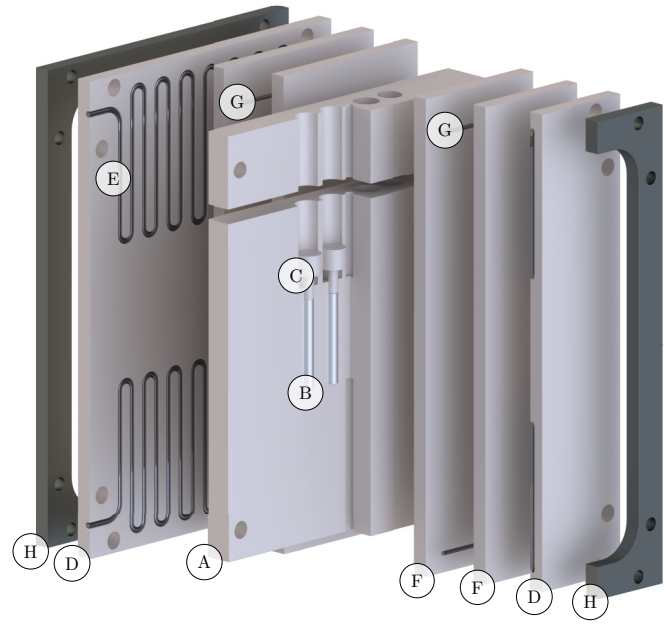

FIG. 1. Exploded view of the sample cell, showing (A) the crucible with (B) samples and (C) pistons, as well as (D) the heat plates, where (E) the heating wire is placed. Between the heating wire and crucible are (F) two extra BN plates with (G) molybdenum wire as separator. The sample cell is held together by (H) the niobium frame. The plates, wires, and frame in front of the crucible, as well as the crucible parts themselves, are cut in the figure to reveal the pistons and samples. The BN plates between the crucible and the heating wires are also cut in the figure to reveal the meandering course of the heating wire.

The temperature is measured at the endpoints of the samples, 12.5 mm from each other, by two sheathed type-K thermocouples with an outer diameter of 1 mm.

The entire sample cell measures 58 × 40 × 24 mm and contains the samples inside the BN crucible, with the BN pistons. On both sides of the BN crucible, BN plates are placed as separators followed by BN plates with molybdenum heating wires and a niobium frame for mechanical stability. An exploded view of the sample cell is shown in Fig. 1.

It has previously been shown that the inclination of the samples in the experimental setup can have a large effect on the measured Soret coefficient due to gravity-induced convection [4]. Therefore, a great amount of care is taken to ensure that the samples are as vertical as possible to reduce this disturbance in addition to using a setup where the cold side was at the bottom, minimizing convective mixing.

Sedimentation of the denser component is not an issue in atomic fluids because the thermal energy is higher than the gravitational potential energy by orders of magnitude [39].

The sample cell is thermally insulated by 3 cm of graphite foam and placed in a water-cooled aluminum container in a vacuum chamber.

For x-ray imaging, we used a microfocus x-ray source (XT9160-TED, Viscom AG, Hannover, Germany) which was operated at 100 kV and 120 μA, and a CdTe detector with a

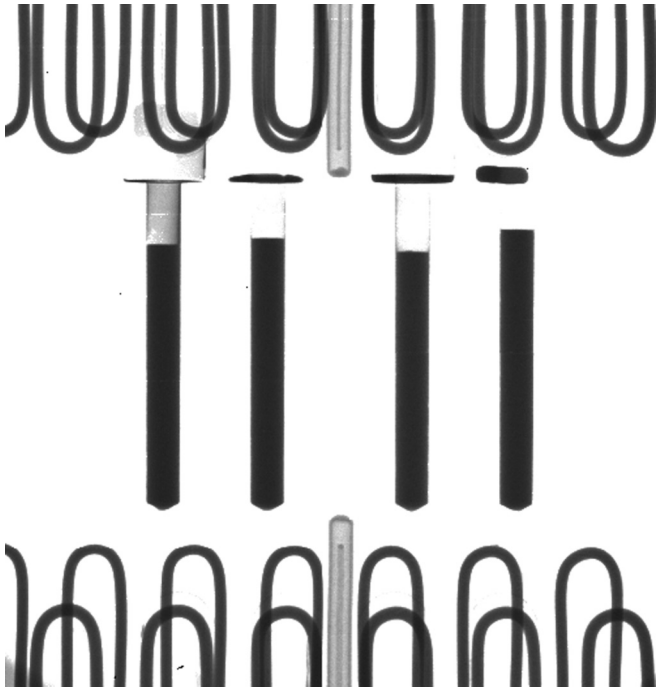

FIG. 2. X-ray radiography (XRR) image of the sample cell, with its four samples, heating wires, and the two thermocouples. The faint white horizontal lines originate from gaps between different parts of the x-ray detector. This image is purposefully darker to render visible thermocouples and heating wires.

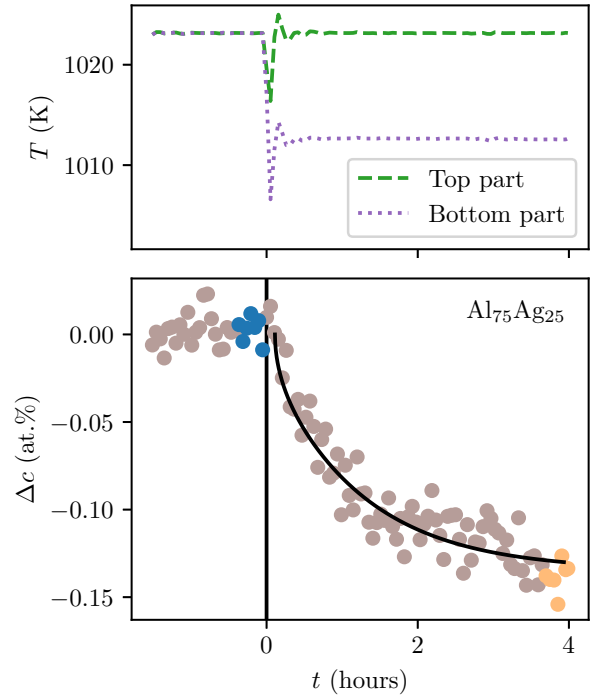

FIG. 3. Concentration difference $\Delta c(t)$ across a sample of $Al_{75}Ag_{25}$, with the temperature measurements at the upper and lower part of the sample shown above. The vertical line indicates when the temperature gradient was initiated. The exponential curve is the fit of Eq. (4) to the experimental data after the temperature gradient had stabilized. The colors indicate the basis for the averaged data used in calculation of the Soret coefficient.

100 μm pixel size (XC-Thor series, Direct Conversion AB, Danderyd, Sweden). With the sample cell located between the source and detector, the resulting images have a resolution of 20 pixels/mm across the sample. The images were filtered by flat-field correction with reference gray images.

B. Experimental procedure

After melting the samples by heating to 1023 K, x-ray images with an exposure time of 1250 ms were recorded at 15 s intervals, one of which can be seen in Fig. 2. After homogenization for ∼2 h in an isothermal state, a temperature gradient of ∼10 Kcm^{-1} was established by switching off the heater at the bottom of the samples.

Two types of sample cells were prepared using four Al–Ag samples each, the first containing two 25 at. % silver ($Al_{75}Ag_{25}$) samples, one 20 at. % ($Al_{80}Ag_{20}$), and one 30 at. % ($Al_{70}Ag_{30}$); the second containing two $Al_{50}Ag_{50}$ samples, one $Al_{55}Ag_{45}$, and one $Al_{45}Ag_{55}$ [40]. In each case, the last two samples are used as references for determining the relation between transmitted x-ray intensity and sample concentration.

The density varies across the sample with temperature due to thermal expansion, affecting the transmittance of x rays. In the case of a small density change, the x-ray transmittance is inversely proportional to the density ρ. Then the transmitted beam intensity difference ΔI across the sample caused by the temperature difference alone is given by

$$\Delta I \approx \bar{I}\frac{\rho_{\mathrm{T}}}{\rho_{\mathrm{L}}}\Delta T, \tag{5}$$

with the average transmitted x-ray intensity through the sample being $\bar{I}$. The temperature-dependent density of the liquid alloy here is given by the linear relation $\rho_{\mathrm{L}} + \rho_{\mathrm{T}}(T - T_{\mathrm{L}})$, where T_{L} is the liquidus temperature of the alloy, ρ_{L} is the density at the liquidus temperature, and ρ_{T} is the change of density per kelvin, using the material parameters from Brillo *et al.* [41]. This must be subtracted from the x-ray images so that the density change is not falsely interpreted as atom migration. This subtraction is done in all data presented in this paper.

The data analysis consists of the following steps: The temperatures are recorded alongside the images. Through software analysis, the pixel ranges containing the samples are determined, and the gray values are extracted and averaged over the width of the sample. The aforementioned density gradient adjustment is performed, the concentration gradient is measured, and the Soret and interdiffusion coefficients are extracted using Eqs. (3) and (4). For Eq. (4), 100 terms of the series are used.

IV. RESULTS

A. Soret coefficient

Figure 3 shows the concentration difference for an $Al_{75}Ag_{25}$ sample over time with the hot end fixed at 1023 K. The figure, displaying the concentration difference of silver between the hot and cold ends of the sample, shows that the silver concentration is reduced in the hot end and increasing

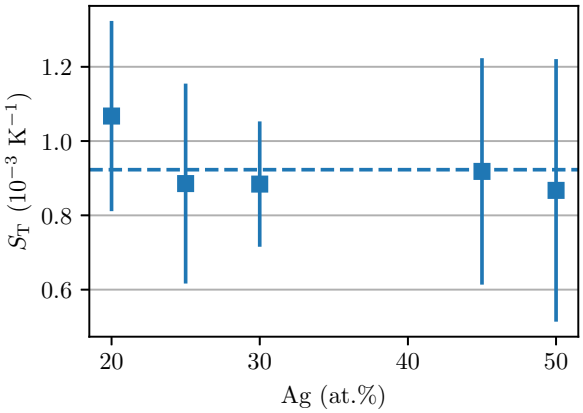

FIG. 4. Soret coefficients accumulated from all experiments, measured at a mean temperature of 1018 K and with temperature differences of ∼10 K. Error bars show one standard deviation for the Soret coefficient for each concentration. The dashed line shows the weighted mean of all our measurements.

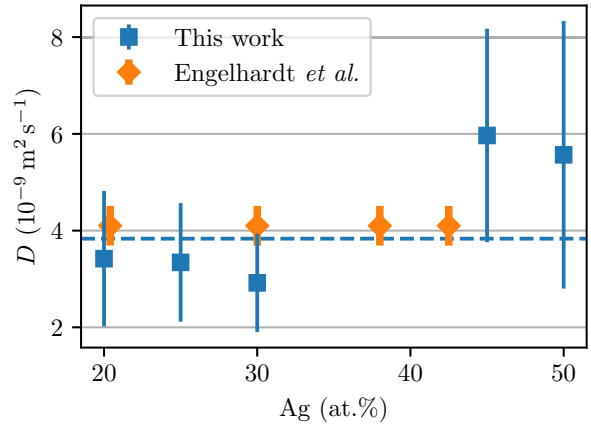

FIG. 5. Interdiffusion coefficients accumulated from all experiments, measured at a mean temperature of 1018 K. Error bars for this paper show one standard deviation for the interdiffusion coefficient for each concentration. The orange diamonds show the data with uncertainty from Engelhardt *et al.* [34], who measured the interdiffusion coefficients using the long capillary method at a temperature of 983 K. The dashed line shows the weighted mean of all our measurements.

at the cold end, meaning that silver migrates to the cold side. Using the concentration gradient data from the nonisothermal equilibrium phase (highlighted on the right in the aforementioned figure) together with the last data of the isothermal phase (highlighted on the left in the aforementioned figure), the Soret coefficient can be calculated directly using Eq. (3).

These experiments were repeated a minimum of five times with each sample cell, allowed by the noninvasiveness of XRR. The averaged Soret coefficient for each composition is presented in Fig. 4. The Soret coefficients show a slight increase for the lowest silver concentration, i.e., $Al_{80}Ag_{20}$, but this increase is within the standard deviation of the measured Soret coefficients of all the $Al_{80}Ag_{20}$ samples and therefore not statistically significant. We thus conjecture that the Soret coefficient is independent of the concentration in the measured range from $Al_{80}Ag_{20}$ to $Al_{50}Ag_{50}$. Weighting for the different uncertainties for each alloy, the averaged Soret coefficient over the entire measured concentration range is found to be $(0.9 \pm 0.3) \times 10^{-3}$ K^{-1}.

B. Interdiffusion coefficient

As the time evolution of the concentration reaching toward equilibrium is available, it is possible to do a least-squares fit of the function describing the time evolution of the concentration given in Eq. (4). From this optimization, the interdiffusion coefficient was calculated.

The interdiffusion coefficient of all experiments is shown in Fig. 5, where they are compared with the measurements of Engelhardt *et al.* [34]. Due to lower contrast across the darker samples of $Al_{55}Ag_{45}$ and $Al_{50}Ag_{50}$, the interdiffusion coefficient for these samples has greater uncertainty than for samples of lower silver concentrations.

V. DISCUSSION

A. Comparison with results from the literature

To the best of our knowledge, there are no previous data on the Soret coefficient for the liquid Al–Ag system. There was, however, a thermomigration experiment on solid Al–Ag with up to 2 at. % silver performed by McKee and Stark [42], measuring a Soret coefficient of -2.0×10^{-3} K^{-1} for a single crystal of $Al_{98}Ag_2$ with the hot end at 923 K, just beneath the liquidus temperature, with silver migrating to the hot end. Thus, our measured Soret coefficient for the liquid alloy has the opposite sign and half the absolute value of the measurements in the solid alloy. By comparison, previous measurements on trace amounts of antimony in silver yielded a Soret coefficient five times higher in the solid state than in the liquid state, with antimony going to the hot side in both cases [24,43]. It has been shown that the measured Soret coefficient is highly dependent on the crystallinity of the solid sample: In the case of solid Al–Cu, the direction of the measured thermodiffusion even reverted with different grain sizes [44]. Any conclusions on the relation between the Soret coefficient in the liquid and solid states of the same alloy are therefore not advisable.

Our measured Soret coefficient is like previous investigations on liquid alloys of Ag–Te by Williams and Philbrook [22], Al–Ni by Sondermann *et al.* [32], and Al–Cu by Bhat [21,26], where the denser element diffused toward the cold side in all cases. The Soret coefficient reported in this paper is also within the same order of magnitude as systems of liquid alkali metal alloys, liquid salts, glass melts, and even several organic compounds [25,45–47].

The interdiffusion coefficient reported in this paper coincides with the Al–Ag measurements of Engelhardt *et al.* [34], who, using the long capillary method at a temperature of 983 K, reported a constant interdiffusion coefficient of $(4.1 \pm 0.4) \times 10^{-9}$ m^{2}s^{-1} for silver concentrations ranging from 20.4 to 42.5 at. %. This agreement further corroborates the measured Soret coefficient itself, as the observed thermodiffusive process evolves at the rate predicted by Eq. (4). The match with the previously published interdiffusion coefficient indicates that the convection in our experiments was negligible.

Equation (4) assumes an instantaneously achieved temperature gradient. Though this is in practice impossible, the time required to reach 90% of the targeted temperature gradient in our setup is ∼3 min, much shorter than the characteristic time for the thermodiffusive process, which is ∼40 min, calculated from the interdiffusion coefficient and the sample length. Therefore, it is assumed that the equation can be applied to describe the time dependence of the concentration gradient in this setup.

While XRR allows for *in situ* measurements, which enables the measurement of interdiffusion coefficients, the small relative difference in concentration results in low contrast and therefore is a limiting factor to the available precision of the measurements. For the experiments with $Al_{75}Ag_{25}$, the total gray value change across the sample is ∼15 gray values, meaning a contrast resolution of ∼0.01 at. %. This gives an uncertainty in the measured Soret coefficient of $0.1 \times 10^{-3}\,\mathrm{K}^{-1}$ in the ideal case. This uncertainty is even larger for the $Al_{50}Ag_{50}$ measurements, where the increased absorption of x rays reduces the contrast by a factor of two and therefore increases the minimum possible uncertainty in the Soret coefficient by the same factor.

It should, however, be noted that the temperature difference in these experiments, which was ∼10 K, is much smaller than many previous works on thermodiffusion in liquid alloys, which use temperature differences often $\gg 100$ K [21,27,28,48]. This reduced temperature difference reduces the heat to be dissipated from the experimental setup, making it more suitable for situations where heat dissipation is a limiting factor, such as on orbital platforms. Additionally, a high-temperature difference between the two ends of the sample gives significantly different interdiffusion coefficients across the sample and therefore impedes the measurement and following comparison of the interdiffusion coefficient. This problem is therefore avoided with a smaller temperature difference.

B. Comparison with predictive models from the literature

Several analytical models for predicting the Soret coefficient in a binary system have been proposed. A model developed specifically for predicting the Soret coefficient in binary liquid alloys was published by Eslamian *et al.* [17]. They modeled the system as an interaction between thermophysical and electronic contributions stemming from the Seebeck effect, resulting in the equation:

$$S_\mathrm{T} = \frac{E_0^\mathrm{vis} - E_1^\mathrm{vis} - (z_1\mathcal{E}_0 - z_0\mathcal{E}_1)c_1 F T}{c_0 T \frac{\partial \mu_0}{\partial c_0}}, \tag{6}$$

where in our case, index 0 denotes silver and 1 denotes aluminum. The component-specific parameters are for component i: E_i^vis the activation energy of viscous flow, z_i the valence of ions, $\mathcal{E}_i$ the thermoelectric power, c_i the mole fraction, and μ_i the chemical potential. Lastly, T is the mean temperature, and F is Faraday's constant. For the calculation of the derivative of the chemical potential, we use the excess Gibbs energy G_E from Witusiewicz *et al.* [33] together with the relations for the chemical potential and activity coefficient γ_i:

$$\mu_i = RT(\ln c_i + \ln \gamma_i), \tag{7}$$

and [49]

$$\ln \gamma_i = \frac{1}{RT}\left[G_\mathrm{E} + (1 - c_i)\frac{\partial G_\mathrm{E}}{\partial c_i}\right], \tag{8}$$

where R is the molar gas constant. Using values for $\mathcal{E}_i$ from Makradi *et al.* [50] and Marwaha and Cusack [51], and E_i^vis from Assael *et al.* [52,53], the model in Eq. (6) predicts a Soret coefficient of $0.45 \times 10^{-3}\,\mathrm{K}^{-1}$ for $Al_{75}Ag_{25}$ at a mean temperature of 1018 K over the sample, which is half of our measured value. There is, however, a considerable uncertainty in the value for the activation energy of viscous flow and in the derivative of the chemical potential, where the corresponding double derivative of G_E amplifies any error in the optimization made to obtain the parameters for G_E.

It should be noted that Eq. (6) is not symmetrical, thus breaking with the very fundamental relationship of the definition of the Soret coefficient in Eq. (3) that $S_{\mathrm{T}1} = -S_{\mathrm{T}0}$ in binary mixtures.

Jafar-Salehi *et al.* [54] developed a model like the model given by Eq. (6), the difference being that the term $c_0\frac{\partial \mu_0}{\partial c_0}$ is developed into a function of mole fraction, density, and temperature. Since their model was developed assuming a dilute mixture, it will not be applied here.

Finally, Hoang and Galliero [13], in a publication where they simulated thermodiffusion in a Lennard-Jones fluid, found that the predictive model by Shukla and Firoozabadi [15] was "the most reasonable" [13] (but still not particularly accurate) model available for fluids. It is given as

$$S_\mathrm{T} = \frac{\frac{U_1}{\tau_1} - \frac{U_0}{\tau_0}}{c_0 T \frac{\partial \mu_0}{\partial c_0}} + \frac{(V_0 - V_1)\left(c_0\frac{U_0}{\tau_0} + c_1\frac{U_1}{\tau_1}\right)}{(c_0 V_0 + c_1 V_1)c_0 T \frac{\partial \mu_0}{\partial c_0}}. \tag{9}$$

Here, the component-specific parameters are for component i: V_i the partial molar volume, U_i the partial molar internal energy, and $\tau_i = E_i^\mathrm{vap}/E_i^\mathrm{vis}$, where E_i^vap is the energy of vaporization. For fluids, U_i is close to the partial molar enthalpy [55], so we again use the excess Gibbs energy from Witusiewicz *et al.* [33] and the fact that the partial molar enthalpy ΔH_i is related to the activity coefficient through [49]

$$\Delta H_i = -RT^2\left(\frac{\partial \ln \gamma_i}{\partial T}\right). \tag{10}$$

For V_i, we assume that it is equal to the molar mass divided by density and obtain those values from Assael *et al.* [52,53]. We use the energies of vaporization from Yaws and Satyro [56]. We then obtain a predicted Soret coefficient of $0.11 \times 10^{-3}\,\mathrm{K}^{-1}$, which differs by an order of magnitude from our measurements.

For both models, the predicted Soret coefficients for all different concentrations are shown in Table I.

Both models discussed here predicted the same sign for the Soret coefficient of liquid Al–Ag alloys as found in our experiments, i.e., correctly predicted the direction of thermodiffusion for the two components in the alloy. However, the numerical values were off by at least a factor of two with respect to our measured values, and the strong concentration dependence predicted by the models was not observed. This

TABLE I. The measured Soret coefficients for the different concentrations, together with the coefficients predicted by the models discussed in this paper. All values are given in units of $10^{-3}\,K^{-1}$. Both the measurements and the calculations had a mean temperature of 1018 K.

	Measured	Eq. (6)	Eq. (9)
$Al_{80}Ag_{20}$	1.1 ± 0.3	0.41	0.09
$Al_{75}Ag_{25}$	0.9 ± 0.3	0.45	0.11
$Al_{70}Ag_{30}$	0.9 ± 0.2	0.46	0.11
$Al_{55}Ag_{45}$	0.9 ± 0.3	0.28	0.06
$Al_{50}Ag_{50}$	0.9 ± 0.4	0.21	0.04

shows that there is still the need for a theory to describe thermodiffusion even in binary atomic liquids.

VI. CONCLUSIONS

The Soret and interdiffusion coefficients of Al–Ag were experimentally determined using a recently developed setup in combination with XRR. The analyzed samples had silver concentrations ranging from 20 to 50 at. % and were measured with the hot end at 1023 K and at a temperature difference of ∼10 K. A Soret coefficient of $(0.9 \pm 0.3) \times 10^{-3}\,K^{-1}$ was determined, which is of the same order of magnitude as previous measurements on similar binary systems. Using experimental data from the literature, models to predict the Soret coefficient were tested. The closest model is off by a factor of two with respect to our measured values. The method of XRR for *in situ* measurements also allows the measurement of the interdiffusion coefficient, which was found to be in accordance with previous interdiffusion measurements on the Al–Ag system, thus indicating that the convection was negligible. Furthermore, using XRR allows several samples to be analyzed simultaneously as well as several times in succession, with relative ease.

ACKNOWLEDGMENTS

The authors would like to thank their institute workshop for help in manufacturing the setup, M. Langer for preparation of samples, and J. Brillo, M. Clozel, B. Reiplinger, and F. Yang for proofreading of the manuscript.

[1] S. Srinivasan and M. Z. Saghir, *Thermodiffusion in Multicomponent Mixtures* (Springer, New York, 2013).
[2] W. Köhler and K. I. Morozov, J. Non-Equilib. Thermodyn. **41**, 151 (2016).
[3] J. K. Platten, M. M. Bou-Ali, P. Costesèque, J. F. Dutrieux, W. Köhler, C. Leppla, S. Wiegand, and G. Wittko, Philos. Mag. **83**, 1965 (2003).
[4] S. A. Mousavi, T. Yousefi, and Z. Saghir, Can. J. Chem. Eng. **95**, 398 (2017).
[5] M. Schraml, T. Triller, D. Sommermann, and W. Köhler, Acta Astronaut. **160**, 251 (2019).
[6] M. Tomaru, T. Osada, I. Orikasa, S. Suzuki, and Y. Inatomi, Microgravity Sci. Technol. **31**, 49 (2019).
[7] B. Cameron Reed, Phys. Perspect. **13**, 161 (2011).
[8] M. Ben Sassi, S. Kaddeche, M. Lappa, S. Millet, D. Henry, and H. Ben Hadid, J. Cryst. Growth **458**, 154 (2017).
[9] J. Lewis and S. Huang, Rev. Sci. Instrum. **34**, 271 (1963).
[10] H.-Y. Hsiao and C. Chen, Appl. Phys. Lett. **94**, 092107 (2009).
[11] C. Q. Ru, J. Mater. Sci. **35**, 5575 (2000).
[12] D.-G. Xie, Z.-Y. Nie, S. Shinzato, Y.-Q. Yang, F.-X. Liu, S. Ogata, J. Li, E. Ma, and Z.-W. Shan, Nat. Commun. **10**, 4478 (2019).
[13] H. Hoang and G. Galliero, Eur. Phys. J. E **45**, 42 (2022).
[14] F. R. Winter and H. G. Drickamer, J. Phys. Chem. **59**, 1229 (1955).
[15] K. Shukla and A. Firoozabadi, Ind. Eng. Chem. Res. **37**, 3331 (1998).
[16] L. J. T. M. Kempers, J. Chem. Phys. **115**, 6330 (2001).
[17] M. Eslamian, F. Sabzi, and M. Z. Saghir, Phys. Chem. Chem. Phys. **12**, 13835 (2010).
[18] U. Sarder, T. Ahmed, W. Y. Wang, R. Kozubski, Z.-K. Liu, I. V. Belova, and G. E. Murch, Philos. Mag. **99**, 468 (2019).
[19] V. Vaibhav, J. Horbach, and P. Chaudhuri, Phys. Rev. E **101**, 022605 (2020).
[20] L. F. Mondolfo, Aluminum–silver system, in *Aluminum Alloys: Structure and Properties* (Butterworth-Heinemann, Oxford, 1976), pp. 213–224.
[21] B. N. Bhat, J. Cryst. Growth **28**, 68 (1975).
[22] R. K. Williams and W. O. Philbrook, J. Electrochem. Soc. **128**, 1034 (1981).
[23] J. M. Brenan and N. Bennett, Earth Planet. Sci. Lett. **298**, 299 (2010).
[24] B. N. Bhat and R. A. Swalin, Z. Naturforsch. **26**, 45 (1971).
[25] S. P. Murarka, T. Y. Kim, M. Y. Hsieh, and R. A. Swalin, Acta Metall. **22**, 185 (1974).
[26] B. N. Bhat, *Thermotransport in Liquid Aluminum-Copper Alloys*, NASA Technical Report, NASA TR R-415 (NASA, Washington, D.C., 1973).
[27] J.-P. Praizey, Int. J. Heat Mass Transf. **32**, 2385 (1989).
[28] J.-P. Praizey, S. Van Vaerenbergh, and J.-P. Garandet, Adv. Space Res. **16**, 205 (1995).
[29] M. Kassemi, S. Barsi, J. I. D. Alexander, and M. Banish, J. Cryst. Growth **276**, 621 (2005).
[30] R. Roşu-Pflumm, W. Wendl, G. Müller-Vogt, S. Suzuki, K.-H. Kraatz, and G. Frohberg, Int. J. Heat Mass Transf. **52**, 6042 (2009).
[31] F. Kargl, E. Sondermann, H. Weis, and A. Meyer, High Temp. High Press. **42**, 3 (2013).
[32] E. Sondermann, F. Kargl, and A. Meyer, Phys. Rev. Lett. **123**, 255902 (2019).
[33] V. T. Witusiewicz, U. Hecht, S. G. Fries, and S. Rex, J. Alloys Compd. **385**, 133 (2004).
[34] M. Engelhardt, A. Meyer, F. Yang, G. G. Simeoni, and F. Kargl, Defect Diffus. Forum **367**, 157 (2016).
[35] J. K. Platten, J. Appl. Mech. **73**, 5 (2006).
[36] J. A. Bierlein, J. Chem. Phys. **23**, 10 (1955).
[37] P. Costesèque, T. Pollak, J. K. Platten, and M. Marcoux, Eur. Phys. J. E **15**, 249 (2004).

[38] A. Mialdun and V. M. Shevtsova, Int. J. Heat Mass Transf. **51**, 3164 (2008).
[39] E. Sondermann, T. Voigtmann, and A. Meyer, Microgravity Sci. Technol. **34**, 93 (2022).
[40] Note that, due to the darkness from the high silver concentration and low contrast, $Al_{45}Ag_{55}$ failed to deliver consistent coefficients. It has therefore been omitted from the results of this paper. It was nevertheless still perfectly valid as a reference for correlating gray value to contrast together with the other samples in the image.
[41] J. Brillo, I. Egry, and J. Westphal, Int. J. Mater. Res. **99**, 162 (2008).
[42] R. A. McKee and J. P. Stark, Acta Metall. **22**, 953 (1974).
[43] W. Biermann, D. Heitkamp, and T. S. Lundy, Acta Metall. **13**, 71 (1965).
[44] R. E. Doerr and J. P. Stark, Metall. Trans. **3**, 2461 (1972).
[45] W. Fuchs and J. Richter, Ber. Bunsenges. Phys. Chem. **86**, 46 (1982).
[46] M. Shimizu, S. Hosoya, T. Kato, J. Matsuoka, H. Kato, M. Nishi, K. Hirao, Y. Shimotsuma, and K. Miura, J. Ceram. Soc. Jpn. **126**, 997 (2018).
[47] S. Hartmann, G. Wittko, F. Schock, W. Groß, F. Lindner, W. Köhler, and K. I. Morozov, J. Chem. Phys. **141**, 134503 (2014).
[48] A. Ott, Science **164**, 297 (1969).
[49] S. M. Walas, Activity coefficients, in *Phase Equilibria in Chemical Engineering* (Butterworth-Heinemann, Oxford, 1985), pp. 165–244.
[50] A. Makradi, H. Chaaba, and J. G. Gasser, Philos. Mag. B **80**, 1727 (2000).
[51] A. S. Marwaha and N. E. Cusack, Phys. Lett. **22**, 556 (1966).
[52] M. J. Assael, K. Kakosimos, R. M. Banish, J. Brillo, I. Egry, R. Brooks, P. N. Quested, K. C. Mills, A. Nagashima, Y. Sato *et al.*, J. Phys. Chem. Ref. Data **35**, 285 (2006).
[53] M. J. Assael, A. E. Kalyva, K. D. Antoniadis, R. M. Banish, I. Egry, J. Wu, E. Kaschnitz, and W. A. Wakeham, High Temp. High Press. **41**, 161 (2012).
[54] E. Jafar-Salehi, M. Eslamian, and M. Z. Saghir, Can. J. Chem. Eng. **92**, 1314 (2014).
[55] P.-A. Artola and B. Rousseau, Phys. Rev. Lett. **98**, 125901 (2007).
[56] C. L. Yaws and M. A. Satyro, in *Thermophysical Properties of Chemicals and Hydrocarbons* (William Andrew, Norwich, 2009), pp. 401–408.